

Surface lattice resonance of circular nano-array integrated on optical fiber tips

Jian Wu(吴坚), Gao-Jie Ye(叶高杰), Xiu-Yang Pang(庞修洋), Xuefen Kan(阚雪芬), Yan Lu(陆炎), Jian Shi(史健), Qiang Yu(俞强), Cheng Yin(殷澄), and Xianping Wang(王贤平)
Citation: Chin. Phys. B, 2023, 32 (**12**): 120701. DOI: 10.1088/1674-1056/acf491
Journal homepage: http://cpb.iphy.ac.cn; http://iopscience.iop.org/cpb

What follows is a list of articles you may be interested in

Damage and recovery of fiber Bragg grating under radiation environment

Shi-Zhe Wen(温世喆), Wei-Chen Xiong(熊伟晨), Li-Ping Huang(黄力平), Zhen-Rui Wang(王镇锐), Xing-Bin Zhang(张兴斌), Zhen-Hui He(何振辉)
Chin. Phys. B, 2018, 27 (**9**): 090701. DOI: 10.1088/1674-1056/27/9/090701

Demonstration of multi-Watt all-fiber superfluorescent source operating near 980 nm

Yankun Ren(任彦锟), Jianqiu Cao(曹涧秋), Hanyuan Ying(应汉辕), Heng Chen(陈恒), Zhiyong Pan(潘志勇), Shaojun Du(杜少军), Jinbao Chen(陈金宝)
Chin. Phys. B, 2018, 27 (**3**): 030703. DOI: 10.1088/1674-1056/27/3/030703

Numerical and experimental analysis of long period gratings in wavelength scale elliptical microfibers

Wa Jin(金娃), Wei-Hong Bi(毕卫红), Guang-Wei Fu(付广伟)
Chin. Phys. B, 2017, 26 (**10**): 100702. DOI: 10.1088/1674-1056/26/10/100702

Digital coherent detection research on Brillouin optical time domain reflectometry with simplex pulse codes

Hao Yun-Qi (郝蕴琦), Ye Qing (叶青), Pan Zheng-Qing (潘政清), Cai Hai-Wen (蔡海文), Qu Rong-Hui (瞿荣辉)
Chin. Phys. B, 2014, 23 (**11**): 110703. DOI: 10.1088/1674-1056/23/11/110703

Spectral analysis of the UFBG-based acousto–optical modulatorin *V-I* transmission matrix formalism

Wu Liang-Ying (吴良英), Pei Li (裴丽), Liu Chao (刘超), Wang Yi-Qun (王一群), Weng Si-Jun (翁思俊), Wang Jian-Shuai (王建帅)
Chin. Phys. B, 2014, 23 (**11**): 110702. DOI: 10.1088/1674-1056/23/11/110702

Surface lattice resonance of circular nano-array integrated on optical fiber tips

Jian Wu(吴坚)[1,†], Gao-Jie Ye(叶高杰)[2], Xiu-Yang Pang(庞修洋)[1], Xuefen Kan(阚雪芬)[3], Yan Lu(陆炎)[3], Jian Shi(史健)[4], Qiang Yu(俞强)[1,5], Cheng Yin(殷澄)[2,‡], and Xianping Wang(王贤平)[4]

[1] *College of Advanced Interdisciplinary Studies, Nanhu Laser Laboratory, Hunan Provincial Key Laboratory of High Energy Laser Technology, National University of Defense Technology, Changsha* 410073, *China*

[2] *College of Internet of Things Engineering, Hohai University, Changzhou* 213022, *China*

[3] *School of Transportation Engineering, Jiangsu Shipping College, Nantong* 226010, *China*

[4] *Jiangxi Key Laboratory of Photoelectronics and Telecommunication, College of Physics and Communication Electronics, Jiangxi Normal University, Nanchang* 330022, *China*

[5] *i-Lab & Key Laboratory of Nanodevices and Applications & Key Laboratory of Nanophotonic Materials and Devices, Suzhou Institute of Nano-Tech and Nano-Bionics, Chinese Academy of Sciences, Suzhou* 215123, *China*

(Received 16 April 2023; revised manuscript received 22 August 2023; accepted manuscript online 29 August 2023)

As metallic nanoparticles are arranged to form a 2D periodic nano-array, the coupling of the localized surface plasmonic resonance (LSPR) results in the well-known phenomenon of surface lattice resonances (SLRs). We theoretically investigate the SLR effect of the circular nano-array fabricated on the fiber tips. The difference between the 2D periodic and circular periodic arrays results in different resonant characteristics. For both structures, the resonant peaks due to the SLRs shift continuously as the array structures are adjusted. For some specific arrangements, the circular nano-array may generate a single sharp resonant peak with extremely high enhancement, which originates from the collective coupling of the whole array. More interestingly, the spatial pattern of the vector near-field corresponding to the sharp peak is independent of the polarization state of the incidence, facilitating its excitation and regulation. This finding may be helpful for designing multifunctional all-fiber devices.

Keywords: fiber tip, lattice resonance, metallic nanoparticles, vector field

PACS: 07.60.Vg, 41.20.Jb, 61.46.Df **DOI:** 10.1088/1674-1056/acf491

1. Introduction

Taking advantages of small size, light weight, multiple functions, low insertion loss, fiber tip devices become attractive candidates for beam shaping,[1] remote sensing,[2] optical manipulating,[3] imaging and signal processing.[4–6] Due to the advances in the fiber optics and micro-nano fabrication technique, great efforts have been devoted to integration of the 2D materials or 3D structures on the optical fiber tips for developing multifunctional all-fiber photonic networks. However, these patterned fiber tips suffer from disadvantages such as complicated fabricating process and short light–matter interaction depth.[7,8] Consequently, it is quite desirable to find a device with new resonance mechanism, which can be easily excited and incorporated on the fiber tips at low cost.

Surface lattice resonances (SLRs)[9] originate from the interaction of light field with nanoparticle arrays,[10] which manifest themselves as drastic narrow plasmon resonances.[11,12] Conventionally, these particles are arranged in periodic 1D or 2D arrays, and the width of the corresponding plasmonic resonance can be as narrow as 12 nm due to the coupling between the localized surface plasmon resonance (LSPR) of individual nanoparticles.[13] In addition, the SLRs have other advantages including high field enhancement, convenient light extinction, and effective light–matter interaction. Thus SLR effect of the plasmonic arrays have broad potential in ultrasensitive detection,[14] photovoltaic devices,[15] optical communication, and metamaterials,[16] etc.

Instead of the transitional symmetry of the 2D periodic array, a circular periodic nano-array with rotational symmetry is adopted in this work as the resonant device. The excitation of the SLR effect is investigated based on a simple coupled-dipole approximation. Particularly, a single and rather sharp resonant peak can be excited via some specific circular array structures. Such resonance is due to the optimum coupling between all the dipole components, resulting in an extremely high intensity of the concentrated near field. As shown in the concrete example of a circular nano-array with six particles in the later section, the enhancement factor of the sharp peak is at least five (two) orders under radially (azimuthally) polarized incidence in comparison with other SLRs peaks. More importantly, it is found that the near-field pattern corresponding to the sharp peak is independent of the polarization state of the excitation. It is worth emphasizing that all the results are obtained via analytical models, thus our findings is theoretically credible. Recently, optical complex fields

†Corresponding author. E-mail: wujian15203@163.com

‡Corresponding author. E-mail: yinch@hhu.edu.cn

© 2023 Chinese Physical Society and IOP Publishing Ltd

with spatially inhomogeneous distributions of the polarization states and optical singularities are subjects of increasing interest, which introduce extra degrees of freedom to enable new applications.[17–19] This proposed resonant structure provides a rather simple approach to generate optical complex near fields with enhanced local intensity and rich topological features on the stage of fiber tips. The light–matter interaction can be significantly enhanced via the excitation of the SLR effect. Furthermore, the dimensions of optical fibers match well with the typical area that can be patterned with the electron-beam lithography (EBL), which is suitable to produce the particle nano-array onto the fiber tips. The proposed model may be attractive in designs of all-fiber photonic devices at low cost.

2. Analytical model

The circular nano-array of identical metallic particles is invariant under certain rotation transformation. The key factor behind the SLRs excitation is that each particle experiences identical driving fields due to the incident light and the light scattered by all the other particles in the array.[13] Since the coaxial adjustment between the array and the incident field is crucial for the excitation of the resonance, the tip of an optical fiber offers a rather natural and convenient stage. Figure 1(a) shows the schematic diagram of the circular nano-array integrated on the fiber tip, where N identical metallic particles with the same orientation are fabricated on the endface of the fiber core. Figure 1(b) demonstrates the radial and azimuthal modes in the fiber structure, i.e., the fundamental TM_{01} and TE_{01} modes. The excitation of the circular array requires vector modes carrying spatial distributed polarization state with rotational symmetry. Such modes can be written as a linear combination of the TM_{01} and TE_{01} modes, which qualify as an orthonormal basis. The schematic diagram of the array design is plotted in Fig. 1(c), where the vector $\boldsymbol{R}_i$ denotes the position of the ith particle P_i. Set the cartesian coordinates of the first particle to be $(R,0)$, then the coordinates of the ith particle P_i are simply $(R\cos\frac{2\pi(i-1)}{N}, R\sin\frac{2\pi(i-1)}{N})$. Since we focus on the SLR effect of the array structure, the metallic particles are simplified to homogeneous ellipsoids, whose semi-axes are referred as a, b, and c, respectively. The quasistatic polarizability approximation is applied to describe the metallic nanoparticles, which is only valid for small particle size.[13] Modified long-wavelength approximation can be utilized for larger particles.[20] As shown in Fig. 1(c), a local cartesian coordinate system (x_i, y_i) is defined for each particle P_i, where the x_i axis coincides with the minor axis of the ellipsoid and the y_i axis aligns with the major axis. Furthermore, the orientation of each particle is described by the angle θ between the major axis and the unit vector in the radial direction, which is defined in the range $-\pi/2 < \theta < \pi/2$.

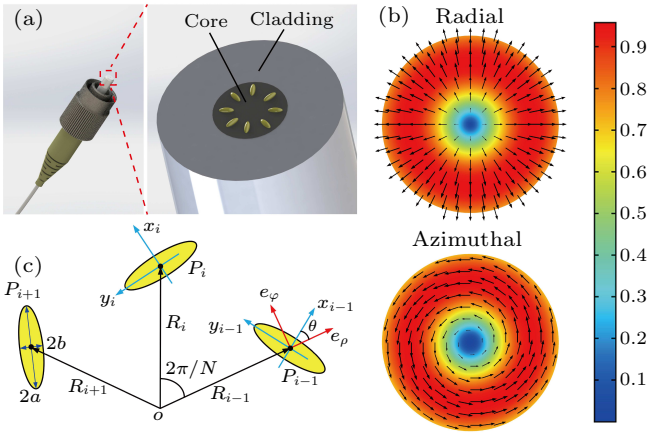


Fig. 1. Circular nano-array integrated on the optical fiber tip. (a) Schematic view of the metallic nanoparticle circle fabricated on the endface of fiber core. (b) The normalized electrical field and polarization distribution of the radial and azimuthal modes in the fiber core. (c) The geometrical model of the circular nano-array.

Now we can represent each particle by its polarizability α_x and α_y in its local cartesian coordinate system (x_i, y_i) as

$$\alpha_{x,y} = 4\pi\varepsilon_{\mathrm{m}} ab^2 \frac{\varepsilon_{\mathrm{p}} - \varepsilon_{\mathrm{m}}}{3\varepsilon_{\mathrm{m}} + 3L_{x,y}(\varepsilon_{\mathrm{p}} - \varepsilon_{\mathrm{m}})}, \tag{1}$$

where ε_{p} and ε_{m} represent the relative permittivity of the particle and the surrounding medium, respectively, and $L_{x,y}$ is the shape factor.[21] Without loss of generality, the electrical field of the optical fiber mode with rotational symmetry can be written in a vector form in the cylindrical coordinate system (ρ, φ) as

$$\boldsymbol{E}_{\mathrm{inc}} = \begin{bmatrix} E_\rho \\ E_\phi \mathrm{e}^{\mathrm{i}\varphi} \end{bmatrix}, \tag{2}$$

where E_ρ and E_φ represent the amplitudes of the radial and azimuthal components, and ϕ is the phase difference. For further usage, the incident field should be rewritten in the local coordinate system (x_i, y_i) of individual particle as $\begin{bmatrix} E_x^{\mathrm{inc}} & E_y^{\mathrm{inc}} \end{bmatrix}^{\mathrm{T}}$. Excited by the external field, a dipole momentum $\boldsymbol{p}_i$ will be induced for every particle, which can be divided into two parts, i.e.,

$$\boldsymbol{p}_i = \boldsymbol{p}_i^{\mathrm{inc}} + \boldsymbol{p}_i^{\mathrm{dipole}}, \tag{3}$$

where the first term is due to the external incident field, and the second term is induced by the radiation from other dipoles in the nano-array. For the second term, an array factor matrix S can be introduced, whose matrix element S_{ij} describes how the p_j component of all the other particles affects the p_i component of the targeted particle. Based on the above derivation, we are ready to solve the dipole momentum $\boldsymbol{p}_i$ as a matrix equation

$$\boldsymbol{p}_i = \begin{bmatrix} p_x \\ p_y \end{bmatrix} = \mathrm{EF} \begin{bmatrix} 1 - S_{yy} & S_{xy} \\ S_{yx} & 1 - S_{xx} \end{bmatrix} \begin{bmatrix} \alpha_x E_x^{\mathrm{inc}} \\ \alpha_y E_y^{\mathrm{inc}} \end{bmatrix}, \tag{4}$$

with the enhancement factor (abbreviated as EF)

$$\mathrm{EF} = \frac{1}{(1 - S_{xx})(1 - S_{yy}) - S_{xy}S_{yx}}. \tag{5}$$

The matrix element S_{ij} of the factor matrix is

$$S_{ij} = \frac{1}{4\pi\varepsilon_m}\sum_{i=2}^{N}\frac{\mathrm{e}^{\mathrm{i}kr_l}}{r_l}\hat{n}_i \times\left\{k^2(\hat{n}_l\times\hat{n}_{lj})\times\hat{n}_l+[3\hat{n}_l(\hat{n}_l\cdot\hat{n}_{lj})-\hat{n}_{lj}]\left(\frac{1}{r_l^2}-\frac{\mathrm{i}k}{r_l}\right)\right\}, \quad i,j\in[x,y], \tag{6}$$

where r_l is the distance from the targeted dipole p_1 to the lth dipole p_l, and $\boldsymbol{r}_l = r_l\hat{n}_l$ is the corresponding vector. $\hat{n}_i$ denotes the unit vector of the ith component of the targeted dipole p_1, and $\hat{n}_{lj}$ denotes the unit vector of the jth component of the lth dipole p_l. Equation (6) shows that the array factor matrix S summaries the four kinds of coupling mechanisms between the different dipole components of the array particles. The element S_{xx} and S_{yy} denote the coupling between the x-components, and y-components, respectively. The intercoupling between the x- and y-components are attributed to the elements S_{xy} and S_{yx}. The two expressions (4) and (5) are the key results of this study, which are obtained analytically owing to the rotational symmetry of both the incident mode and the particle array. The details for the analytical model are provided in the supporting materials.

Generally, the EF depends on the incident wavelength, the particle polarizability, the array radius, the particle number and the particle orientation, while the latter three parameters determine the structure of the circular nano-array. Since we are extremely interested in how the array arrangement influences the SLRs, we focus on the array parameters in this work. The influence of the incident wavelength and the particle polarizability can be found in the Supporting materials. The SLRs may occur when the EF approaches infinity, whilst its denominator in Eq. (5) approaches zero. Thus the SLRs are influenced by all the coupling mechanisms in a rather complicated way, and all the parameters may affect the resonance feature. In the later sections, concrete examples are presented to investigate the physics behind the SLRs of the circular nano-array and the induced optical complex fields.

3. Simulations and discussions

This section is based on direct simulation of the above analytical model.[22,23] The particles used in the simulations are silver prolate spheroid ($a > b = c$), whose major and minor axes are $a = 60$ nm and $b = c = 25$ nm, respectively. The incident wavelength is $\lambda = 632.8$ nm, and the relative permittivity of silver is based on the Drude model, with plasma frequency $\omega_p = 1.4\times10^{15}$ Hz and the damping constant $\Gamma = 3.2\times10^{13}$ Hz.[24]

Since the metallic particles are already fixed, the EF is predominantly determined by the structural parameters. Figure 2(a) compares the EF of three circular arrays with different particle number N, and the SLRs illustrate themselves as the gray strips. Similar to the SLRs in a 2D periodic array,[25] the resonant positions of the circular array shift continuously as the structural parameters are adjusted. Two gray regions are marked out as I and Ⅱ, corresponding to the two cases of $\theta = 0^\circ$ and $\theta = 90^\circ$, respectively. Consider the schematic diagram in Fig. 2(a), and note that the resonant radius for case I is smaller than the case Ⅱ, so it is clear that in case I the coupling between opposite particles takes the leading role, while in case Ⅱ the coupling between adjacent particles dominates. For more general case that $0^\circ < \theta < 90^\circ$, these two kinds of coupling mix together. A rather interesting case is shown in Fig. 2(b), where a single point-like resonant peak with much larger EF is observed at position ($\theta = 29^\circ$, $R = 86$ nm). We will refer to such resonant behavior as sharp peak of SLRs for short. Three points are labeled as P1, P2 and P3 in Fig. 2(b), and each point represents a specific structural arrange of the circular nano-array. Thus point P1 represents the unique structure that generates the sharp peak, while the other two points correspond to the usual SLR effect.

The near fields of the array radiation under the radial and azimuthal modes are compared in Fig. 2(c) for the above selected structural arrangements in Fig. 2(b). A few statements are available in this stage. Firstly, the electrical field intensity is significantly enhanced for the sharp peak at P1 in comparison with the other two points. The simulation shows that the EF at P1 is at least five (two) order higher for the radially (azimuthally) polarized excitation.[17] Secondly, the light patterns corresponding to points P2 and P3 vary when the spatial polarization distribution of the incidence differs, while the light patterns of the sharp peak seem to be invariant. Since these two incident fields form an orthonormal basis, the above demonstrations show that the SLR effect can be excited easily using arbitrary mode with rotational symmetry, and enhanced near field can be effectively produced at the endface of an optical fiber by the integrated circular nano-array.

However, for some circular nano-array arrangement the sharp peak cannot be observed. The simulations in Fig. 3 confirms this statement, where the sharp peaks can only be observed when particle number N equals 6 or 7. In the case of $N = 5$, the EF is larger when the orientation of the array particle is radial, indicating that the coupling between adjacent particles dominates. In the case of $N = 8$, the EF is larger when the orientation of the array particle is azimuthal, so the enhancement can be mainly attributed to the coupling between opposite particles. However, no sharp peak is observed for these two cases. In comparison of the cases of $N = 6$ and $N = 7$, it is clear that the peak position shifts to large orientation angle as the particle number increases. More examples of the sharp peak can be found in the supporting materials.

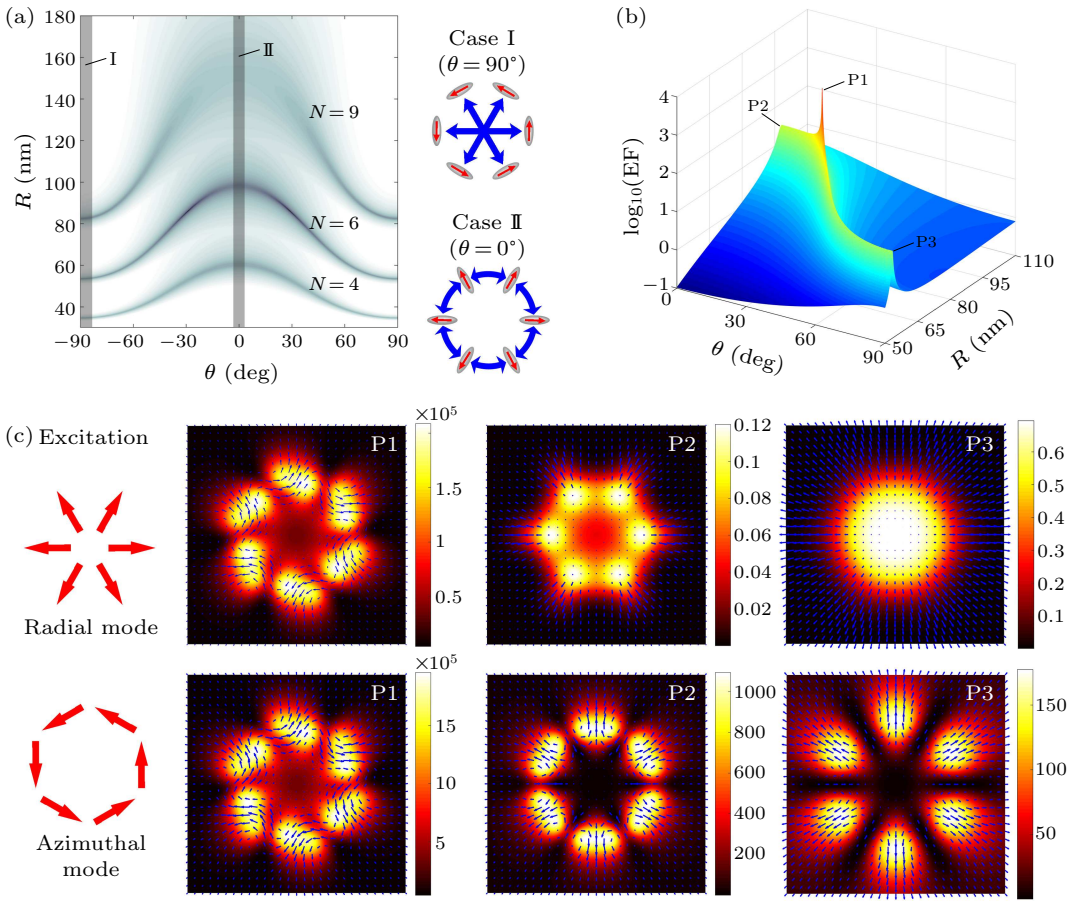


Fig. 2. (a) Comparison of SLR effect of circular particle arrays with different particle number N. Two extreme cases are marked as I and II, where the individual particle are perpendicular ($\theta = 90°$) or parallel ($\theta = 0°$) to the radial direction. Schematic illustrations of the two different coupling mechanisms between the array particles are also displayed by blue arrows corresponding to cases I and II, respectively. (b) The EF of the $N = 6$ array as a function of array radius R and particle orientation θ. Three points are marked out as P1, P2 and P3 for further investigation. (c) The intensity and transverse flux (arrows) of the near fields of the particle arrays under the excitation of the radial or azimuthal fiber modes. The observation plane is 50 nm away from the fiber tips, and arbitrary unit is applied. The simulation area is $2R \times 2R$.

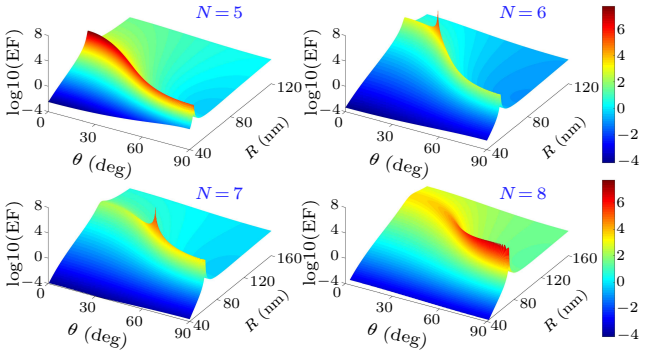


Fig. 3. The shift of the single resonant peak as a function of the particle number of the array.

One of the most interesting characteristics of the sharp peak resonance is that the field distributions seem to be independent of the excitation mode. As shown in Fig. 2(c), the two electrical field distributions are identical for structure P1 under orthogonal fiber mode excitation, except that the intensities are different. It can be helpful for our intuition to reminder that these two modes can work as an orthonormal basis to build up rotational symmetric incidence with arbitrary spatial polarization distribution. Given the specific geometric design, the sharp peak of the SLRs may be excited to generate vector near-field with similar intensity and polarization distributions. It is even possible to use an ordinary fiber mode without rotational symmetry owing to the high coupling efficiency and high EF, but this hypothesis needs to be further verified by practical experiments.

Figure 4 simulates the evolution of the spatial patterns of the sharp peak at different propagation distances. A comparison with other SLR effect can be found in Fig. S3 of the supporting materials. The radiation due to the arrayed dipoles of the metallic particles is localized, whose intensity decreases to only 10^{-3} after propagating for hundred-nanometer distance in our illustration. Thus the field is tightly concentrated near the plane of the array, which facilitates the light–matter interaction at the fiber tips. At short distance, the light pattern is composed of several dipole fields corresponding each particle, which gradually merge together at longer distances due to the interference. Multiple polarization singularities and transverse

flux zeros can be found, which move to infinite or annihilate in pairs with opposite topological index during propagation. Finally, for longer propagation distance, there exists only a single C-point that coincides with a single transverse flux zero at the center of the spatial pattern. These fixed patterns of the sharp peak can be applied in various engineering fields such as optical manipulating, sensing, and signal processing. Lastly, it is necessary to point out that the practical nanoparticle fabricated by present technique would not be a perfect ellipsoid. Given that the wavelength is larger than the particle's dimension, this work can still be applied to analyze the resonance of the circular nano-array effectively.

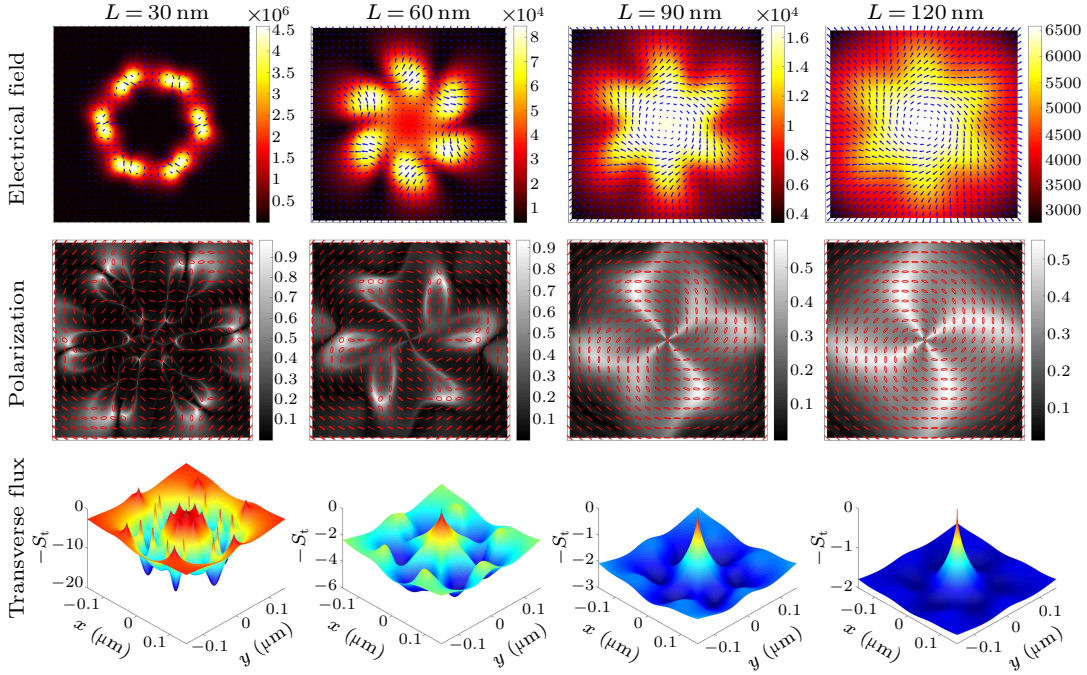


Fig. 4. The evolution of the vectorial near fields of a resonant circular particle arrays ($N = 6$, $R = 86$ nm and $\theta = 29°$) at different propagation distances $L = 30$ nm, $L = 60$ nm, $L = 90$ nm, and $L = 120$ nm, respectively. The top row shows the electrical field intensity and the transverse flux (arrows), while the middle row shows the local polarization ellipses (red circles) and the ellipticity. The simulation area is $2R \times 2R$. The bottom row shows the distribution of the zero points in the transverse flux map, where the inverted vertical axis is applied so that the zero points illustrate themselves as peaks.

4. Conclusions

The resonant excitation of the SLR effect via metallic circular nano-arrays is theoretically analyzed on the platform of fiber tips. The analytical model with clear physical interpretations is derived via the quasistatic polarizability approximation. For specific geometric arrangements, the SLRs form a sharp resonant peak, which yields an enhanced near-field with fixed spatial pattern. The high coupling efficiency guarantees the high enhancement of the localized vector field with rich topological characteristics. Thus the proposed structures can be designed specifically to manipulating the spatial distribution of the optical beams via polarization, phase and intensity at ease.

Acknowledgments

The authors thank to Professor Su and Dr. Luo at Hohai University for their fruitful discussions on data processing and computational simulation.

This work was supported by the National Natural Science Foundation of China (Grant No. 12174085), the Fundamental Research Funds for the Central Universities (Grant No. B220202018), the Changzhou Science and Technology Program (Grant No. CJ20210130), and CAS Key Laboratory of Nanodevices and Applications (Grant No. 21YZ03).

References

[1] Principe M, Consales M, Micco A, Crescitelli A, Castaldi G, Esposito E, La Ferrara V, Cutolo A, Galdi V and Cusano A 2017 *Light: Sci. Appl.* **6** e16226
[2] Zhang J, Chen S, Gong T, Zhang X and Zhu Y 2016 *Plasmonics* **11** 743
[3] Berthelot J, Aćimović S S, Juan M L, Kreuzer M P, Renger J and Quidant R 2014 *Nat. Nanotechnol.* **9** 295
[4] Liu M, Yin X, Ulin-Avila E, Geng B, Zentgraf T, Ju L, Wang F and Zhang X 2011 *Nature* **474** 64
[5] Gan X, Zhao C, Wang Y, Mao D, Fang L, Han L and Zhao J 2015 *Optica* **2** 468
[6] Chen J H, Zheng B C, Shao G H, Ge S J, Xu F and Lu Y Q 2015 *Light: Sci. Appl.* **4** e360
[7] Xiong Y and Xu F 2020 *Adv. Photon.* **2** 064001
[8] Chen J H, Xiong Y F, Xu F and Lu Y Q 2021 *Light: Sci. Appl.* **10** 78
[9] Shi Y, Dong Y, Sun D and Li G 2022 *Chin. Phys. B* **31** 14217
[10] Zhu J, Wang X, Wu X, Su Y, Xu Y, Qi Y, Zhang L and Yang H 2020 *Chin. Phys. B* **29** 114204
[11] Michaeli L, Keren-Zur S, Avayu O, Suchowski H and Ellenbogen T 2017 *Phys. Rev. Lett.* **118** 243904
[12] Kravets V G, Kabashin A V, Barnes W L and Grigorenko A N 2018 *Chem. Rev.* **118** 5912
[13] Humphrey A D and Barnes W L 2014 *Phys. Rev. B* **90** 075404

[14] Sreekanth K V, Alapan Y, ElKabbash M, Ilker E, Hinczewski M, Gurkan U A, De Luca A and Strangi G 2016 *Nat. Mater.* **15** 621
[15] Liu W, Miroshnichenko A E, Neshev D N and Kivshar Y S 2012 *Phys. Rev. B* **86** 081407
[16] Manjappa M, Srivastava Y K and Singh R 2016 *Phys. Rev. B* **94** 161103
[17] Rui G, Zhan Q and Cui Y 2015 *Sci. Rep.* **5** 13732
[18] Yang Y, Wu L, Liu Y, *et al.* 2020 *Nano Lett.* **20** 6774
[19] Dorrah A H and Capasso F 2022 *Science* **376** eabi6860
[20] Moroz A 2009 *J. Opt. Soc. Am. B* **26** 517
[21] Bohren C F and Huffman D R 2008 *Absorption and Scattering of Light by Small Particles* (New York: John Wiley & Sons)
[22] Ouyang W H, Liu J B, Lai W S, Li J H and Liu B X 2023 *Chin. Phys. B* **32** 036101
[23] Zhang Z, Yuan J, Qiu S, Zhou G, Zhou X, Yan B, Wu Q, Wang K and Sang X 2023 *Chin. Phys. B* **32** 034208
[24] Cai W and Shalaev V M 2010 *Optical Metamaterials* (Berlin: Springer)
[25] Shi Y, Xiong Lei, Dong Y, Sun D and Li G 2022 *Chin. Phys. B* **31** 014217